VCAN Canonical Splice Site Mutation is Associated With Vitreoretinal Degeneration and Disrupts an MMP Proteolytic Site

Peter H. Tang,[1,2] Gabriel Velez,[1,3] Stephen H. Tsang,[4] Alexander G. Bassuk,[5] and Vinit B. Mahajan[1,2]

[1]Byers Eye Institute, Omics Laboratory, Department of Ophthalmology, Stanford University School of Medicine, Palo Alto, California, United States
[2]Veterans Affairs Palo Alto Health Care System, Palo Alto, California, United States
[3]Medical Scientist Training Program, University of Iowa, Iowa City, Iowa, United States
[4]Bernard and Shirlee Brown Glaucoma Laboratory, Department of Pathology and Cell Biology, Department of Ophthalmology, College of Physicians and Surgeons, Columbia University, New York, New York, United States
[5]Department of Pediatrics, University of Iowa, Iowa City, Iowa, United States

Correspondence: Vinit B. Mahajan, Omics Laboratory, Byers Eye Institute, Department of Ophthalmology, Stanford University School of Medicine, Palo Alto, CA 94304, USA; vinit.mahajan@stanford.com.

PHT and GV are joint first authors.

Submitted: August 31, 2018
Accepted: November 29, 2018

Citation: Tang PH, Velez G, Tsang SH, Bassuk AG, Mahajan VB. *VCAN* canonical splice site mutation is associated with vitreoretinal degeneration and disrupts an MMP proteolytic site. *Invest Ophthalmol Vis Sci*. 2019;60:282–293. https://doi.org/10.1167/iovs.18-25624

Purpose. To gain insight into the pathophysiology of vitreoretinal degeneration, the clinical course of three family members with Versican Vitreoretinopathy (VVR) is described, and a canonical splice site mutation in the gene encoding for versican (*VCAN*) protein was biochemically analyzed.

Methods. A retrospective chart review, human eye histopathology, Sanger DNA sequencing, protein structural modeling, and in vitro proteolysis assays were performed.

Results. The proband (II:1), mother (I:2), and younger sibling (II:2) suffered retinal degeneration with foveal sparing and retinal detachments with proliferative vitreoretinopathy, features that were confirmed on histopathologic analysis. All affected members carried a heterozygous adenine to guanine variant (c.4004-2A>G) predicted to result in exon 8 skipping or the deletion of 13 amino acids at the beginning of the GAGβ chain (VCAN p.1335-1347). This deleted region corresponded to a putative MMP cleavage site, validated using fluorescence resonance energy transfer (FRET)-based proteolysis assays. Proteomic network analysis identified 10 interacting partners in the human vitreous and retina linked to retinal detachment and degeneration.

Conclusions. VVR causes significant ocular disease, including retinal detachment and retinal dystrophy. The intronic *VCAN* mutation removes an MMP cleavage site, which alters versican structure and results in abnormal vitreous modeling. Disruption of a versican protein network may underlie clinicopathologic disease features and point to targeted therapies.

Keywords: versican, wagner disease, erosive vitreoretinopathy, VCAN, genetics, MMP-2, MMP-9, gelatinase, extracellular matrix, vitreous, retinal detachment

Erosive vitreoretinopathy (EVR) and Wagner disease are classically described as separate entities, but recent genetic studies revealed both are due to autosomal dominant mutations in the *VCAN* gene (Online Mendelian Inheritance in Man #118661).[1–4] This gene is localized to chromosome 5q13-q14 and encodes for an extracellular matrix (ECM) chondroitin sulfate proteoglycan called versican, the exact role of which is not well understood.[5] Both Wagner disease and EVR are extremely rare, with 14 pedigrees (with >250 individuals) having been described.[2–11] Patients with Wagner disease can exhibit vitreous syneresis, an optically empty vitreous, equatorial avascular vitreous veils, mild to moderate myopia, cortical cataracts, abnormal retinal vessel architecture (inverted papilla), ectopic fovea, perivascular pigmentation and sheathing, slowly progressive chorioretinal atrophy, and retinoschisis and/or retinal detachment (RD).[12–14] Along with these findings, EVR patients also exhibit progressive nyctalopia, visual field constriction, and loss of rod–cone function on ERG recording.[1,2,8] Some patients with *VCAN* mutations exhibit prominent spontaneous uveitis; however, the mechanism is not well understood.[6,15] Thus, it may be helpful to view both conditions as existing on a spectrum ranging from mild (Wagner disease) to severe (EVR) phenotypes. In the current study, we have termed this collective spectrum of clinical findings as Versican Vitreoretinopathy (VVR).

Turnover of versican through proteolytic processing appears to play an important role in the physiologic structure of tissues, including the vitreous. Proteolytic cleavage of versican by matrix metalloproteinases (MMPs) and A Disintegrin and Metalloproteinase with Thrombospondin motifs (ADAMTS) proteases[16–18] is a critical step in the process of ECM modeling, particularly during embryonic development. Early on, versican-bound hyaluronic acid forms a loose hydrated matrix that allows for rapid modeling and morphogenesis.[19] Versican cleavage facilitates the compaction and sculpting of the ECM in versican-rich tissues.[19] Physiologic versican cleavage is not just degradative—proteolytic processing is highly regulated and can result in the formation of bioactive cleavage products. For

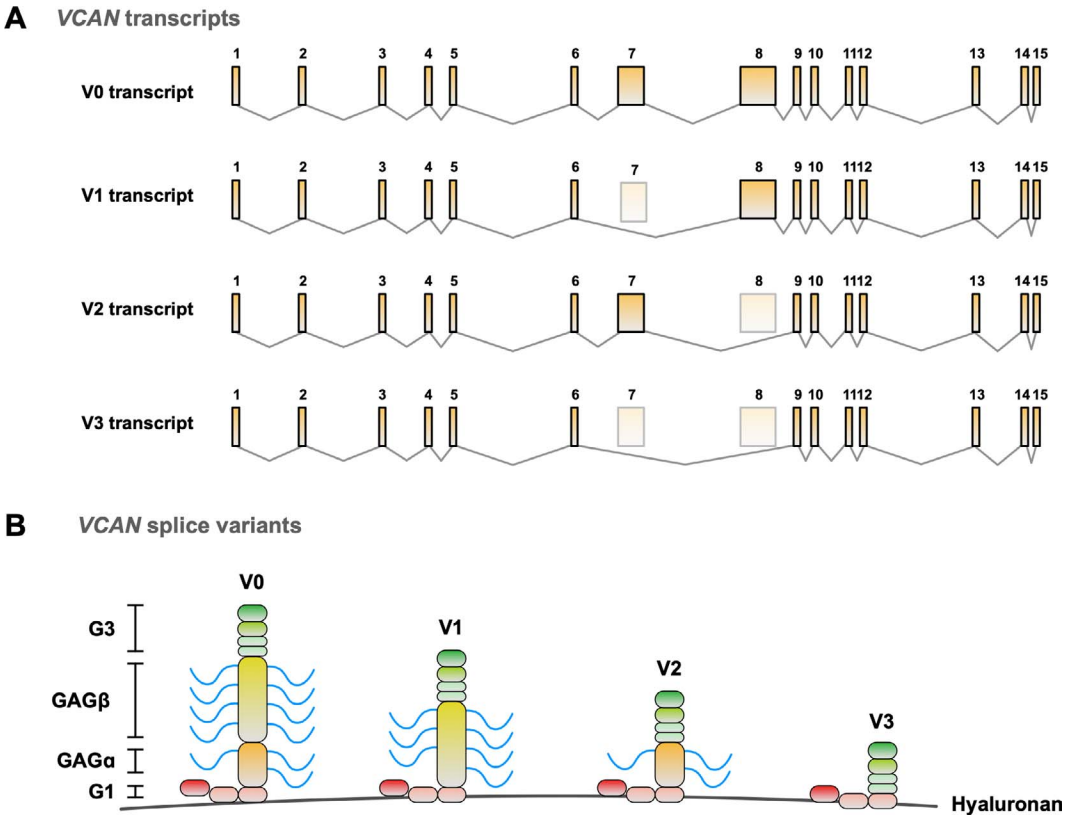

FIGURE 1. *VCAN* transcripts. (**A**) Graphic representation of *VCAN* transcripts. The V0 and V1 transcripts contain exon 8, which encodes for the GAGβ chain. (**B**) Graphic representation of the *VCAN* splice variants. The G1 domain binds versican to the hyaluronan network.

example, ADAMTS-mediated processing of versican results in the formation of a 49-kDa functional product, termed versikine, which facilitates apoptosis in coordination with ECM turnover.[18,19] It is unclear whether additional bioactive fragments are generated. Although the mechanisms for versican processing in the eye are poorly understood, it is hypothesized that dysregulation of these pathways may result in pathologic matrix modeling in the vitreous.[19,20] The role of versican in eye development is further supported by changes in VCAN protein expression in the developing mouse retina and optic nerve, although its significance remains to be delineated.[21] Furthermore, the *Cspg2/Vcan* gene was identified as a Pax6 transcriptional target in the developing mouse lens.[22] In addition to facilitating organization of the vitreous gel, the normal hyaluronan network may serve to sequester proteins in the vitreous. Abnormal matrix modeling could potentially release growth factors and proteins that can impact retinal function. A parallel can be drawn to Marfan syndrome, where mutations in the gene encoding fibrillin-1 (FBLN-1) disrupt its ability to sequester TGFβ leading to a dysregulated TGFβ signal transduction that causes the clinical manifestations, such as RD.[23] Thus, proper processing of versican appears to play a critical role in maintaining the structural integrity of the vitreous.

Disruption of versican structure and its interactions with binding partners could account for key clinical features of VVR. Four isoforms of versican exist (termed V0, V1, V2, and V3; RefSeq IDs: NP_004376.2, NP_001157569.1, NP_001157570.1, and NP_001119808.1, respectively; Fig. 1A).[8] Several known pathologic *VCAN* mutations have been shown to cause skipping of exon 8 during transcription, decreasing the expression of V0 and V1 transcripts, which have higher amounts of chondroitin sulfite side chains compared with the V2 and V3 transcripts (Fig. 1B).[3,24] The canonical *VCAN* splice site mutation c.4004-2A>G is located in a hotspot of other intronic alleles demonstrated to cause VVR.[7,9,11,25] These intronic alleles introduce a cryptic splice acceptor site that leads to a 39-base pair (bp) deletion in exon 8, thereby deleting 13 amino acids in the GAGβ chain. Similarly, heterozygous exon 8 deletions (whole or partial deletions) were also associated with typical Wagner disease in two families.[4] It is therefore hypothesized that deletion of these 13 amino acids (either by whole or partial deletion of exon 8) would have deleterious effects on versican structure and function. The overall hypothesized result is a decrease in the ability of versican to interact with the ECM and cell surface proteins, leading to ocular diseases, such as uveitis and VVR.[8,10] In this report, we further elucidate the characteristics of VVR by describing its clinical and histopathologic phenotype, confirming the *VCAN* c.4004-2A>G mutation in a pedigree of northern European ancestry, and revealing the functional effect of the gene mutation on its protein structure. Finally, using network analysis of protein–protein interactions in the vitreous proteome, we link versican protein effectors to the VVR clinical phenotype.[26,27]

METHODS

Study Approval

The study was approved by the institutional review boards at respective universities and adheres to the tenets set forth in the Declaration of Helsinki. Informed consent was obtained from study participants. A chart review of clinical exams was performed.

Investigative Ophthalmology & Visual Science

DNA Sequencing

DNA sequencing and analysis was performed as previously described.[28] Briefly, genomic DNA from patients was isolated from peripheral blood lymphocytes per standard methods. The entire sequence of *VCAN* (15 exons) was amplified by PCR using pairs of primers that were designed based on the published consensus sequences. Direct sequencing of the PCR-amplified products was analyzed by the Genwize Company (South Plainfield, NJ, USA).

Histologic Analysis

The enucleated eye was fixed in 4% paraformaldehyde solution for 24 hours, washed with PBS, dehydrated using a series of increasing ethanol solution and xylene, embedded in paraffin, sectioned, and mounted on silane-coated slides. Deparaffinized sections were stained with hematoxylin-eosin. Sections were then mounted with cover slip and underwent microscopic analysis and image acquisition.

Cleavage Site Prediction

Proteolytic cleavage sites were predicted with CleavPredict software (Sanford Burnham Medical Research Institute, La Jolla, CA, USA)[29] on the V0 versican primary sequence (NP_004376.2) using default parameters. The analysis returned 28 putative cleavage sites in the VCAN GAGβ chain (residues 1336–3089). Putative cleavage sites were organized by their respective position weighted matrix (PWM) score calculated by CleavPredict. These sites were further filtered by matching their sequence to the classical gelatinase (MMP-2 and MMP-9) substrate recognition motif, which preferentially contains a leucine or methionine in the P1′ position.[30] This filtering returned 13 putative MMP-2 sites, among which was VCAN p.1335-1344 (PWM score = 2.38). Results of this analysis are summarized in Supplementary Table S1.

Docking Calculations

Docking calculations were performed using the limited structure of VCAN p.1335-1344 in AutoDock VINA with a three-dimensional interaction grid of 96Å × 96Å × 96Å around the human MMP-2 catalytic domain structure (PDB: 1QIB).[31] Partial charges were added to the grid using the AMBER03 parameter set. A total of 25 runs were completed generating multiple clusters of receptor-ligand conformations. Binding energies for each cluster were calculated using the equation in VINA: $\Delta G_{bind} = RT\ln K_{bind}$. PyMOL generated all structural images.

MMP Proteolysis Assay

Purified recombinant human pro–MMP-2 (AnaSpec, Fremont, CA, USA) was activated by incubation with 1 mM 4-aminophenylmercuric acetate (APMA) in a buffer containing 50 mM Tris-HCl (pH 7.5), 200 mM NaCl, 5 mM $CaCl_2$, 1 μM $ZnCl_2$, 0.05% Brij35, and 1 mg/mL BSA at 37°C for 1 hour. Proteolytic activity was measured by cleavage of fluorescence resonance energy transfer (FRET)-tagged peptide substrates (Supplementary Table S2; AnaSpec). All FRET peptides contained 5-FAM/QXL dye/quencher pairs. Activated MMP-2 (50 ng per reaction) was incubated with peptide substrate (to 20 μM) at 37°C for 1 hour. Proteolytic activity was measured as change in raw fluorescence units (ΔRFU; $\lambda_{exc} = 490$, $\lambda_{em} = 520$ nm) at 2-minute intervals on a fluorimetric plate reader (Tecan Spark, Männedorf, Switzerland). The concentration of 5-FAM released during the experiment was calculated based on a fluorescence standard curve of 5-FAM-PL concentrations (2 nM to 5 μM). VCAN p.1335-1347 hydrolysis by the recombinant human MMP-9 catalytic domain (residues 112–445) was tested using the same conditions. Kinetic parameters were calculated by direct fitting to the Michaelis-Menten equation in GraphPad Prism 7 (La Jolla, CA, USA).

Network Analysis

Network analysis was performed to identify known versican and MMP-2 binding partners in the human retina and vitreous proteome.[27,32] The list of total retinal, RPE-choroid, and vitreous proteins from our previously published datasets was queried in NetworkAnalyst using the STRING 10.5 search feature with filtering for experimentally validated interactions and manual curation (confidence score cutoff of >0.9).[33,34] This generated a network containing 7050 nodes (proteins) and 38,096 edges (interactions). The resulting network was visualized in Cytoscape 3.5.1 (National Institute of General Medical Sciences, Bethesda, MD, USA) and binding partners of versican and MMP-2 were selected to generate a subnetwork for further analysis.[35]

Results

Clinical Phenotypes

The proband (II:1, Figs. 2A–H) was a 44-year-old male who presented for new flashes in the left eye (OS) after slowly declining vision in both eyes (OU) for many years (Figs. 2A–H). His best corrected visual acuity (BCVA) was 20/300 in the right eye (OD) and 20/500 in OS, as measured by Snellen. There was vitreous matrix degeneration, a far peripheral tractional RD in OS (Figs. 3A, 3B), and fibrosis over the anterior peripheral retina and thin epiretinal membranes in the macula. There was no anterior chamber or vitreous cell/flare noted on clinical examination. Goldmann visual fields showed ring scotomas with foveal sparing. Since age 19, he exhibited areas of extensive sheathing of the major arcade vessels, midperipheral atrophy of the retinal pigment epithelium (RPE), and pigment clumping with drusen-like deposits within the macula OU. A full body bone scan did not reveal any skeletal abnormalities, and ERG testing showed decreased scotopic and photopic responses OU. By age 32, the patient developed visually significant cataracts and underwent uneventful phacoemulsification with intraocular lens insertion OU.

The symptomatic peripheral tractional RD OS was an indication for surgery. Meticulous scleral depressed fundus exam showed vitreous bands and tractional membranes over the peripheral retina and vitreous base with a superior-nasal tractional RD; however, similar to his mother (discussed below), a retinal tear (RT) was not identified. Thus, he was treated with primary placement of a circumferential #42 scleral buckle secured with a #70 sleeve and indirect laser demarcation. Postoperatively, the RD receded, and the retina remained attached at the 1-year follow-up visit.

The proband's mother (I:2, Figs. 2I–L), was a 65-year-old female who initially presented at age 29 with a chronic appearing inferior peripheral RD OS (Figs. 2L, 3C). Three years later she was found to have asymptomatic superior temporal subretinal fluid in OD without an identifiable RT along with the presence of visually significant cataracts OU. By age 34, she underwent lensectomy with combined scleral buckle and pars plana vitrectomy (PPV) OU. She remained aphakic OU, and her BCVA was measured to be 20/20 OD and 20/25 OS; however, this declined to 20/200 OD and 20/500 OS over the next 3

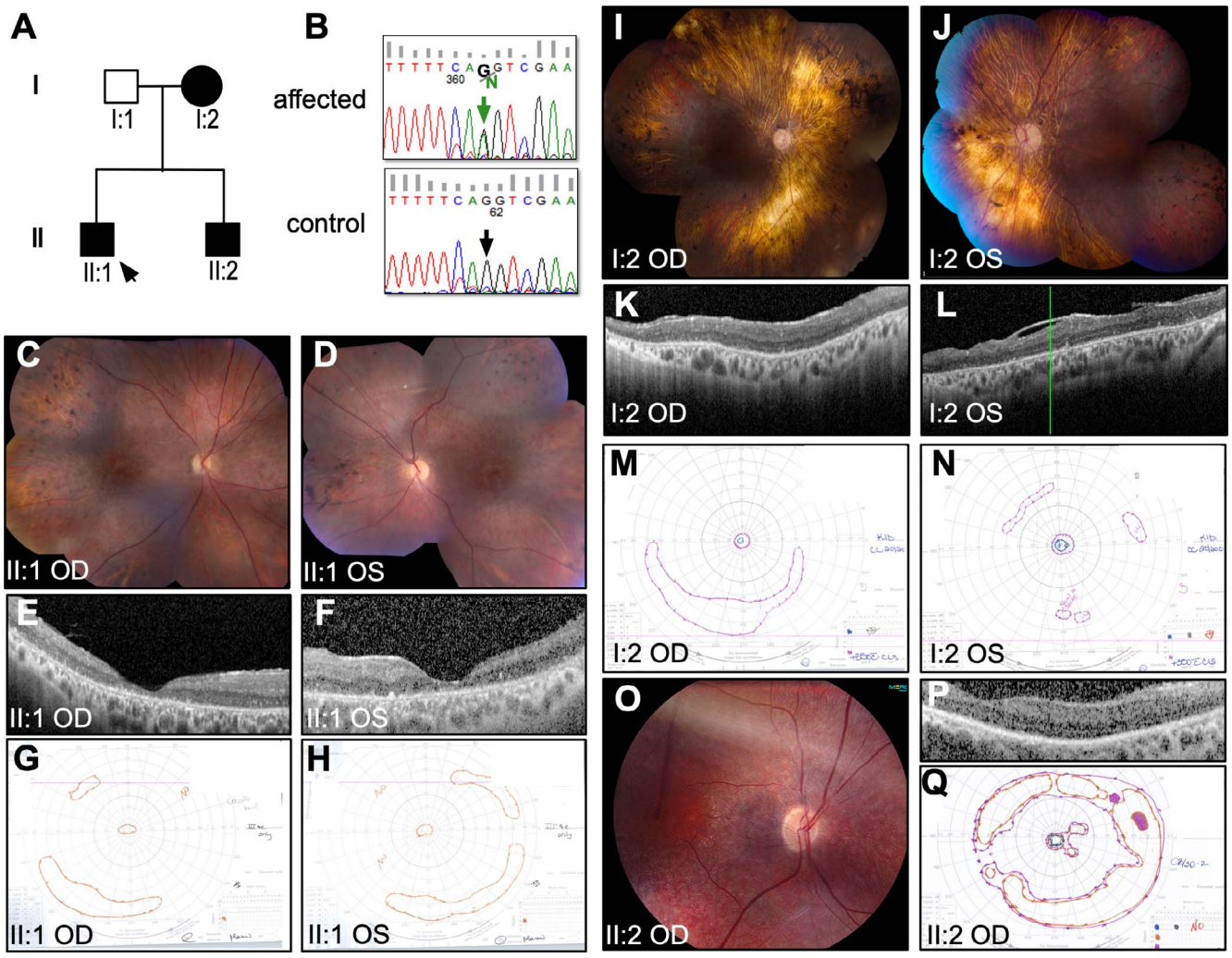

Figure 2. Clinical imaging. Proband (II:1). Family pedigree shown with *arrow* indicating proband (**A**). Sanger sequence analysis of exon 8 of affected individual (**B**, *top*) compared with control (**B**, *bottom*). Color montage fundus photos of OD (**C**) and OS (**D**) showing regions of vascular attenuation and peripheral pigmentary changes. Optical coherence tomography (OCT) imaging of the macula of OD (**E**) and OS (**F**) indicating generalized retinal atrophy. Goldmann perimetry of OD (**G**) and OS (**H**) indicating significant scotomas throughout with peripheral islands of vision. Mother (I:2). Color montage fundus photos from mother in the OD (**I**) and OS (**J**) showing significant vascular attenuation, peripheral pigmentary changes, and regions of choroidal atrophy. OCT imaging of the macula of mother from the OD (**K**) and OS (**L**) indicate generalized retinal atrophy along with formation of epiretinal membrane in OS. Goldmann perimetry from mother in OD (**M**) and OS (**N**) indicate significant scotomas with peripheral islands of vision. Sibling (II:2). Fundus photo of the posterior pole from OD of sibling (**O**) indicate vascular attenuation with pigmentary changes. OCT imaging of macula of OD from sibling indicate significant retinal atrophy (**P**). Goldmann perimetry from sibling indicate significant central scotoma with preservation of peripheral islands of vision (**Q**).

decades with peripheral pigmentary degeneration and the appearance of mild vitreous cell. Goldmann visual fields showed dense ring scotomas with mild foveal sparing. Her retinas remained attached OU.

A 39-year-old male sibling (II:2, Figs. 2M–Q) had an extensive ophthalmic surgical history beginning at age 7 when he presented with a superior bullous RD OS from a single superior RT (Fig. 3D). After multiple interventions, including placement of a scleral buckle, cryoretinopexy, PPV, and the use of intraocular gas, the retina developed proliferative vitreoretinopathy (PVR) that led to multiple re-detachments of the retina and unsuccessful surgical intervention. Ultimately, observation was elected due to poor visual prognosis, and by age 19, his BCVA in the OS deteriorated to no light perception (NLP). Over the next 2 decades, the vision in OD eventually degraded to LP due to significant pigmentary degeneration of the retina with progressive retinal atrophy over decades. Goldmann visual field showed a ring scotoma with foveal sparing. Eventually, the OS became more painful with the development of mild vitreous inflammatory cells, and at age 40 the patient underwent OS enucleation.

Histopathology

The eye (II:2) specimen was sent for histopathologic analysis (Fig. 4). Evaluation of the cornea revealed a degenerative pannus with band keratopathy. Centrally, there was an absence of Descemet membrane along with diffuse endothelial cell loss and secondary stromal edema. Furthermore, a diffuse dystrophic calcification on the posterior surface of the Descemet membrane was noted along with neovascularization of the angle causing subsequent closure and flattening of the anterior chamber. Focal ossification of the anterior chamber and signs of chronic iritis were likely due to multiple prior surgeries. Posteriorly, an exudative and tractional total RD with severe retinal atrophy and gliosis was present. The retinal vasculature

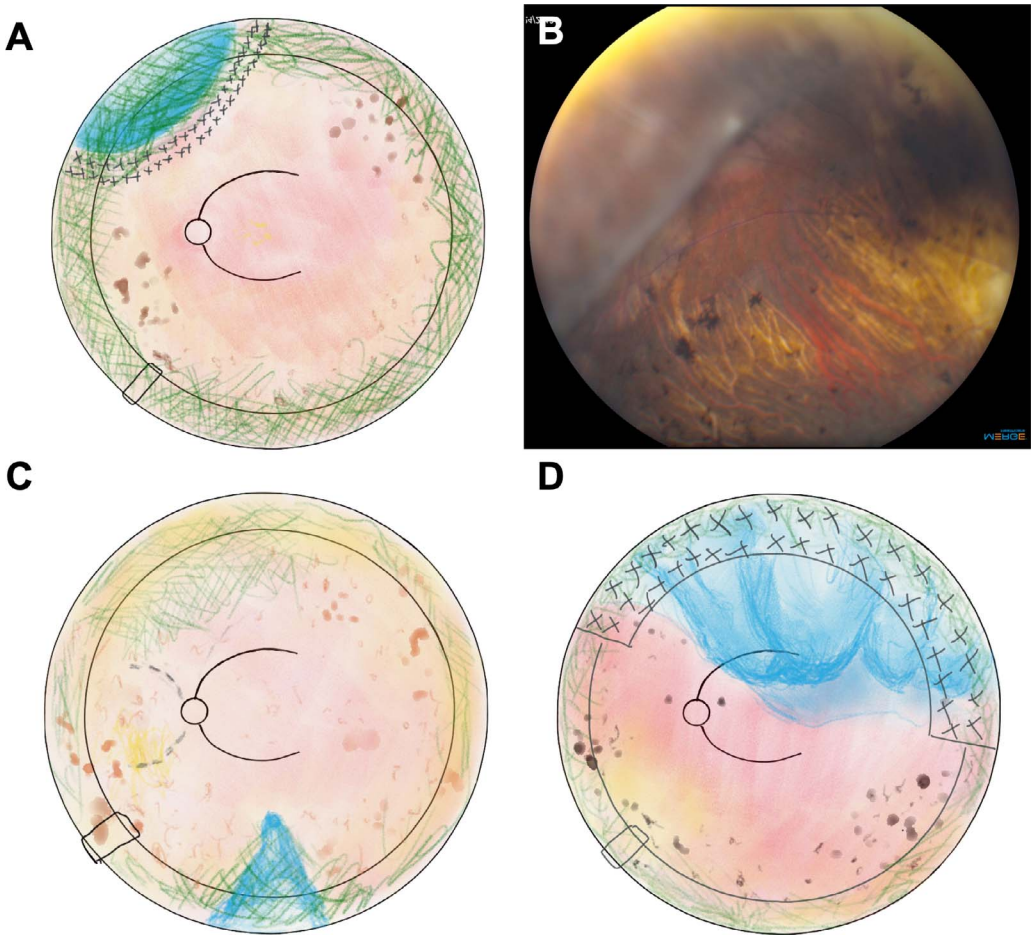

FIGURE 3. Surgical drawings of the fundus. Drawings of the fundus were made at the time of diagnosis of retinal detachments. The proband (II:1) had a retinal detachment in the far peripheral region of the superior nasal quadrant OS (**A**), which is confirmed with fundus photo of the detachment (**B**). The mother of the proband (I:2) had a far peripheral inferior retinal detachment (**C**). The sibling of the proband (II:2) had a bullous superior retinal detachment in OS (**D**).

demonstrated hyalinization, and occasional cystoid spaces and subretinal ossification were observed throughout. There was migration of the RPE into the neurosensory retina, often surrounding areas of retinal vasculature, with osseous metaplasia of the RPE and severe optic nerve atrophy. The RPE was atrophic and the sclera demonstrated a large cystoid space in the region of the equator consistent with the presence of a scleral buckle. These findings, along with the familial presentation of tractional RD, peripheral RPE changes, vitreous bands, and retinal atrophy observed in the other family members were highly suspicious for an inherited vitreoretinal degenerative process.

Genetic Analysis Reveals Mutation in the *VCAN* Gene

The clinical findings were consistent with EVR, thus family members underwent genetic analysis.[13] Sanger sequencing of the *VCAN* coding sequence was performed, and a heterozygous adenine to guanine variant (c.4004-2A>G) within intron 7 was found in all affected members (Fig. 5A). The unaffected father did not harbor this variant. The mutation was found to disrupt the canonical splice acceptor site of exon 8. An alternative splice acceptor site is situated 39-bp downstream, which elsewhere was shown to result in a 39-bp deletion in transcripts V0 and V1.[9] To understand how this genetic mutation affects protein function and pathophysiology, proteomic and structural modeling analysis were conducted.

VCAN Expression in the Human Eye Correlates With VVR Clinical Pathology

Within the human eye, versican expression has been previously reported in the cornea,[36] RPE, Bruch's membrane, choroid, sclera,[37] ciliary body, and the vitreous humor.[38] Transcriptome analysis of human ocular tissues by other groups have further detected *VCAN* RNA in the adult and fetal cornea, ciliary body, and trabecular meshwork (Table 1).[39,40] We queried our human vitreous and retina proteomics datasets for further analysis.[27,41,42] Versican protein expression was abundant in the vitreous (with highest expression in the vitreous core), RPE-choroid complex, and peripheral retina; however, it was absent within the juxtamacular and foveomacular regions (Table 1).[42] These protein expression patterns corresponded to significant peripheral retinal pathology findings we observed in our family members, including peripheral tractional RDs and pigmentary degeneration with foveal sparing. Although abundant levels of versican protein were detected in the human vitreous proteome, the resolution was not sufficient to discern proteolytic cleavage products.

Investigative Ophthalmology & Visual Science

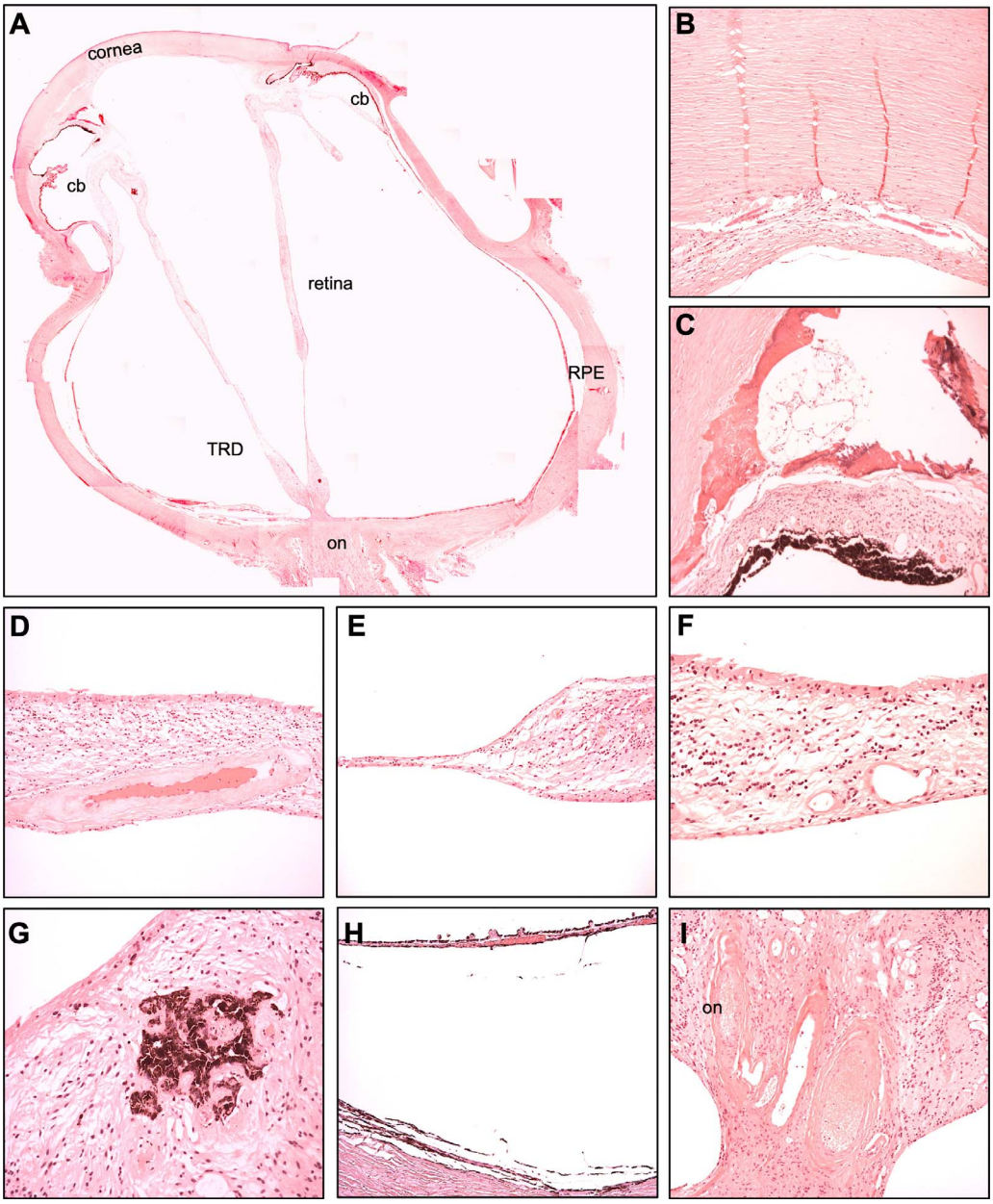

Figure 4. Histopathology. The OD of the sibling (II:2) was aphakic, phthisical, and showed a complete tractional retinal detachment (TRD) at the time of enucleation (**A**). The central cornea demonstrated absence of Descemet's membrane along with diffuse endothelial cell loss with secondary stromal edema (**B**). Neovascularization of the angle with subsequent closure and flattening of the anterior chamber was observed (**C**). The retinal vasculature demonstrated hyalinization (**D**). There was thinning and atrophy of the retina (**E**), cystoid spaces, and subretinal ossification (**E**, **F**) along with pigmentary migration (**G**). The RPE-choroid was thin (**H**). Severe optic nerve atrophy was observed (**I**).

VCAN Canonical Splice Mutation Removes an MMP Proteolytic Site

Versican contains two globular domains, G1 and G3, at the N- and C-terminals, respectively, and two chondroitin sulfate attachment domains centrally (GAGα and GAGβ; Fig. 5B). The N- and C-terminal regions possess multiple motifs that can interact with diverse ECM and cell surface molecules.[43,44] Versican contributes to the overall vitreous structure likely by linking the hyaluronan network to other proteins via its N- and C-terminal domains.[45,46] The clinical phenotypes of our VVR patients indicated an underlying dysregulation of vitreous matrix structure. While previous studies have shown that *VCAN* splice mutations lead to deletions affecting exon 8, little is known about the protein structural effects of GAGβ chain truncation or deletion.[1,4]

We have previously reported that detailed protein structural analysis can provide mechanistic insight into exon mutation function and pathophysiology.[47–52] The 39-bp deletion in our patients caused by the c.4004-2 A>G mutation corresponded to 13 amino acids at the beginning of the versican GAGβ chain (termed VCAN p.1335-1347; NP_004376.2; Fig. 5B). Multiple sequence alignment comparisons of these 13 residues with other species revealed that this region is conserved among mammals (Supplementary Fig. S1A), suggesting that deletion would not be well-tolerated. Thus, we considered potential consequences of deleting the VCAN p.1335–1347 region on protein structure and function.

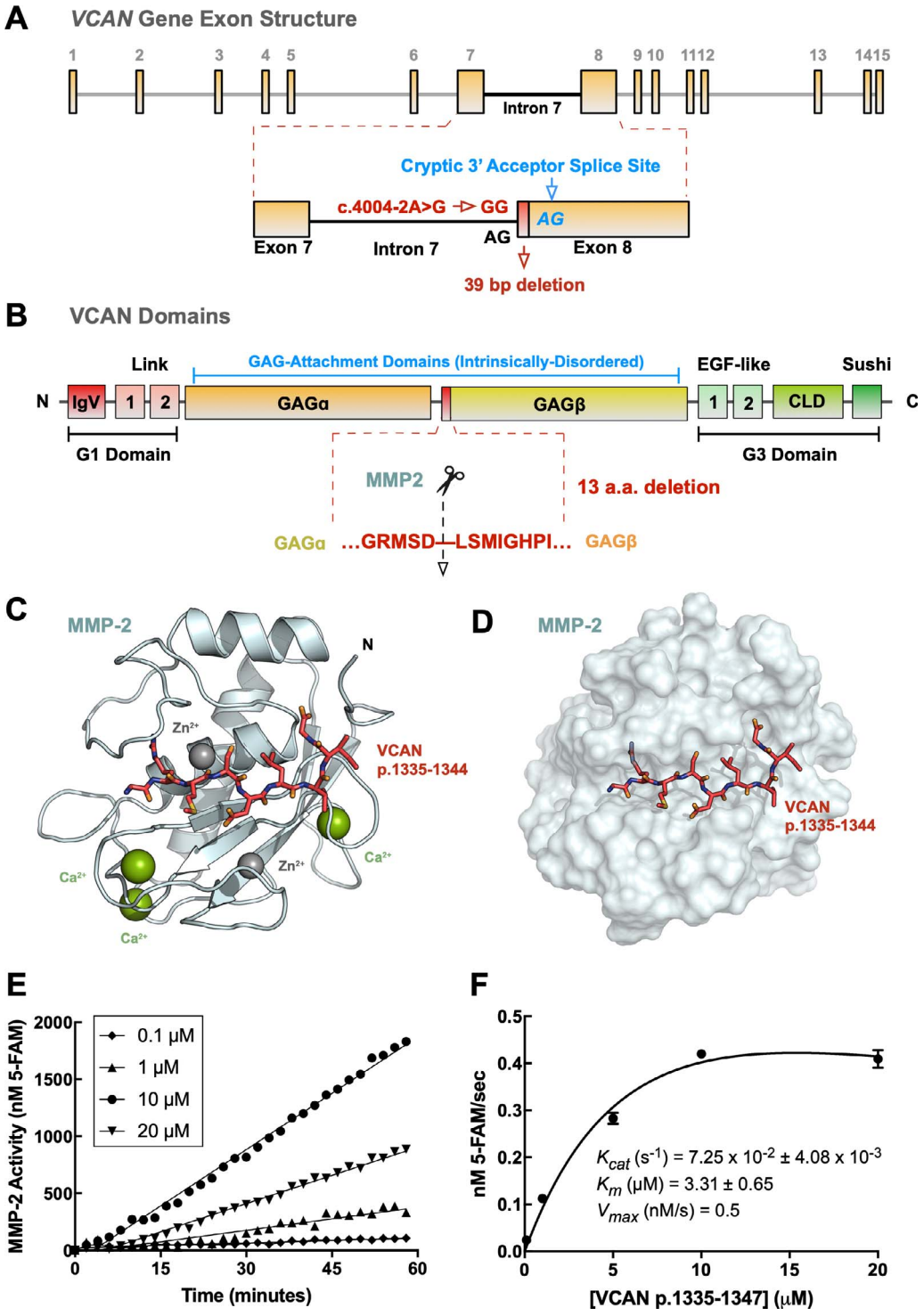

Figure 5. MMP-2 cleaves the p.1335-1347 region of versican. Graphic representation of human *VCAN* gene exon structure showing location of the c.4004-2A>G splice site mutation in intron 7. The c.4004-2A>G creates a cryptic splice acceptor site 39-bp into exon 8 (**A**). Graphic representation of human versican domains (**B**). The VCAN p.1335-1347 region is deleted by the splice variant c.4004-2 A>G. This region corresponds to a putative MMP-2 cleavage site predicted by CleavPredict. In silico docking of VCAN p.1335-1344 to the MMP-2 catalytic domain structure (PDB: 1QIB) yielded a ΔG of 6.33 ± 0.28 kcal/mol across 25 runs in AutoDock VINA (**C**). Surface representation of the VCAN p.1335-1344-MMP-2 complex (**D**). Recombinant MMP-2 proteolytic activity was measured by cleavage of a FRET-tagged substrate (VCAN p.1335-1347; 5-FAM-GRMSDLSMIGHPI-QXL; Supplementary Table S3). Results are displayed as nanomolar product formed per minute time (**E**). Varying concentrations of substrate (to 20 μM) were added to calculate kinetic parameters. The initial velocity (nM 5-FAM/s) of the reaction at each substrate concentration was fit to the Michaelis-Menten equation and kinetic parameters were calculated: $K_{cat} = 7.25 \times 10^{-2} \pm 4.08 \times 10^{-3}$ s^{-1}, $K_m = 3.31 \pm 0.65$ μM, $V_{max} = 0.5$ nM/s (**F**).

Table 1. VCAN Expression in Human Ophthalmic Tissues

Tissue	VCAN/CSPG2	COL18A1	COL2A1	Detection Platform	PMID
Macula	−	+	−	LC-MS/MS	Velez et al.[32]
Fovea	−	+	−	LC-MS/MS	Velez et al.[32]
Peripheral retina	+	+	−	LC-MS/MS	Velez et al.[32]
Vitreous core	+	+	+	LC-MS/MS	Skeie et al.[27]
Vitreous base	+	+	+	LC-MS/MS	Skeie et al.[27]
Vitreous cortex	+	+	+	LC-MS/MS	Skeie et al.[27]
RPE/choroid	+	+	+	LC-MS/MS	Skeie et al.[41]
Ciliary body	+	+	+	RNA-Seq	Carnes et al.[39]
Cornea	+	+	+	RNA-Seq	Carnes et al.[39]
Trabecular meshwork	+	+	+	RNA-Seq	Carnes et al.[39]

LC-MS/MS, liquid chromatography-tandem mass spectrometry.

Because proteolytic cleavage of versican is a critical step in normal ECM modeling, we evaluated vitreous proteases that could cleave VCAN p.1335-1347. Our human vitreous database produced over 140 proteases and MMPs that cleave and degrade ECM proteins to regulate function.[27] We therefore analyzed the versican primary sequence using CleavPredict, a software program that predicts MMP substrate cleavage sites based on position weighted matrices.[29] This analysis predicted the VCAN p.1335-1347 region contained a putative MMP-2 cleavage site that fell within the 13-amino acid region deleted by the splice site mutation (GRMSD—LSMIG; Fig. 4B; Supplementary Table S1). In silico docking of VCAN p.1335-1347 to the MMP-2 catalytic domain structure (PDB: 1QIB) yielded a positive binding energy across 25 runs, further supporting it as a MMP-2 cleavage site ($\Delta G = 6.33 \pm 0.28$ kcal/mol; Figs. 5C, 5D).[31] MMP-2 is highly represented in the human vitreous proteome[27] and is known to cleave versican, but our analysis is the first to identify a specific MMP-2 cleavage site.[17,27]

We validated this putative MMP cleavage site by performing a fluorogenic activity assay.[53] FRET peptides containing 5-FAM/QXL dye/quencher pairs were designed around VCAN p.1335-1347 (Supplementary Table S2). Purified recombinant pro–MMP-2 was activated by incubation with APMA prior to the reaction, and MMP-2 activity was confirmed using a sensitive MMP FRET substrate, QXL-PLGC(Me)HAr-K(5-FAM), and a scrambled negative control (Supplementary Figs. S1B, S1C; Supplementary Table S2).[53,54] Next, the VCAN p.1335-1347 FRET substrate and a scrambled version of its sequence were incubated with active MMP-2. Addition of the enzyme resulted in a significant increase in fluorescence, while the scrambled negative control exhibited no change (Supplementary Figs. S1D, S1E). The kinetic parameters of VCAN p.1335-1347 hydrolysis by MMP-2 ($K_{cat} = 7.25 \times 10^{-2} \pm 4.08 \times 10^{-3}$ s^{-1}, $K_m = 3.31 \pm 0.65$ μM; Table 2) confirm that the c.4004-2A>G variant disrupts an MMP cleavage site at the beginning of the versican GAGβ domain (Figs. 5D, 5E), lending further support to our earlier finding.

We similarly tested VCAN p.1335-1347 hydrolysis by recombinant human MMP-9 catalytic domain (residues 112-445; AnaSpec) to evaluate if this site demonstrated any preference for MMP-2. Consistent with previous observations that gelatinases (MMP-2 and -9) cleave versican, recombinant MMP-9 hydrolyzed VCAN p.1335-1347 in our FRET assay ($K_{cat} = 3.83 \times 10^{-2} \pm 6.03 \times 10^{-3}$ s^{-1}, $K_m = 4.43 \pm 2.18$ μM; Table 2). However, its catalytic efficiency was less than half that of MMP-2, suggesting that this reaction is more favorable for MMP-2 (Table 2). Disruption of this cleavage site globally changes the versican protein structure and may result in the pathophysiology underlying the clinical findings observed in our VVR patients.

Table 2. Kinetic Parameters for VCAN p.1335-1347 Hydrolysis by Human MMPs

Parameter	Human MMP-2	Human MMP-9
K_{cat}, s^{-1}	$7.25 \times 10^{-2} \pm 4.08 \times 10^{-3}$	$3.83 \times 10^{-2} \pm 6.03 \times 10^{-3}$
K_m, μM	3.31 ± 0.65	4.43 ± 2.18
K_{cat}/K_m, $M^{-1}s^{-1}$	2.19×10^4	8.65×10^3
Relative catalytic efficiency	1	0.39

Network Analysis Model

Protein–protein interactions between normally processed versican and other nonstructural proteins within the vitreous could be disrupted by the c.4004-2A>G mutation to the GAGβ domain. Polysaccharide-bound GAG chains contain negative charges that facilitate interactions with positively charged molecules (e.g., growth factors, chemokines, and cytokines).[55] Dysfunction may impact overall vitreoretinal health through mis-sequestration of these proteins,[56] but this process has previously been difficult to model. We performed network analysis of the human vitreous and retinal proteome to generate a model of proteins that can interact with versican.[28] This analysis generated a network containing 7050 nodes (proteins) and 38,096 edges (interactions). Binding partners of versican and MMP-2 were extracted to generate a subnetwork with 28 nodes and 32 edges (Fig. 6).

Deleterious structural consequences on ECM proteins within the vitreous could account for key clinical features.[57] There were seven versican-associated ECM proteins in this network, including FBLN1, FBNL2, fibulin-1 (FBN1), tenascin-R (TNR), glypican-1 (GPC1), bi-glycan (BGN), and aggrecan (ACAN). Organization of these proteins in the vitreous could be affected by abnormal vitreous matrix modeling. Alterations of ECM modeling proteins, including TNR and ACAN, have been observed in animal models of neurodegeneration and retinal ischemia.[58] Retina ischemia can cause retinovascular leakage, which is a precursor to PVR, a key feature of our VVR patients.

Members of our VVR family and other individuals with this disease have shown findings of mild uveitis.[6] We identified CXCL12, a known chemoattractant for T cells and monocytes.[59] Unregulated CXCL12 activity after disruption of versican interaction could trigger inflammatory cell migration into the vitreous and promote a proinflammatory state. We also identified VEGFA, which is associated with pathologic retinal vascular permeability and PVR that can lead to RD.[60–62] Proteolytic degradation of versican in vascular basement membranes has been previously shown to initiate VEGFA-

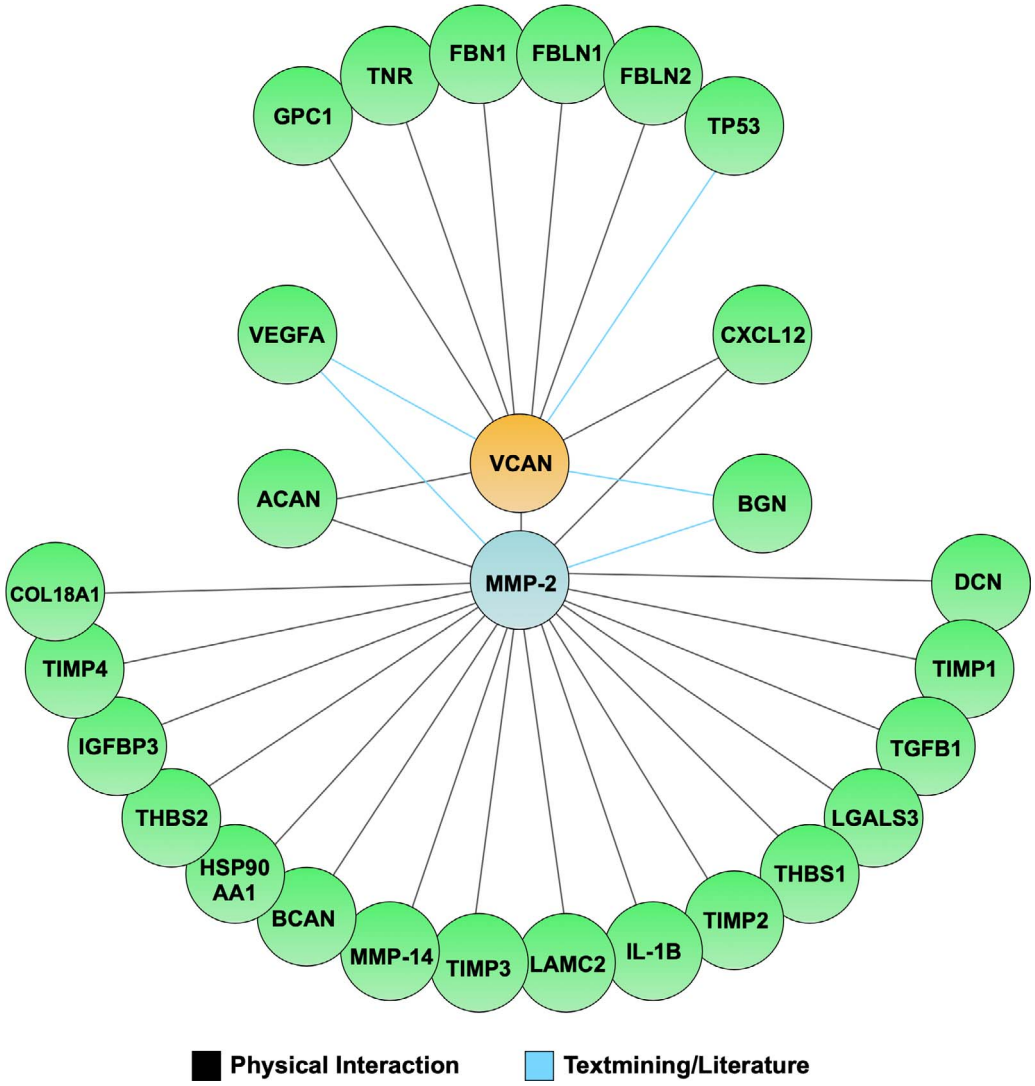

Figure 6. Versican interactors in the retina and vitreous. VCAN/MMP-2 network generated in STRING 10.5 The network contains 28 nodes (proteins) and 32 edges (interactions). Edges represent physical interaction (*black*) or predicted interaction (*cyan*).

induced angiogenesis and vascular leakage.[60] These putative binding partners support the hypothesis that dysregulation of matrix structure in the vitreous may result in the release of sequestered proteins and have pathologic consequences leading to the clinical features of VVR (Fig. 6).

Discussion

Versican is a large chondroitin sulfate proteoglycan that is variably expressed in numerous types of human tissues. Previously, it was shown to function in numerous roles, such as promoting cellular adhesion, migration, proliferation, angiogenesis, and inflammation.[63,64] Upregulation of versican has been implicated in malignant cancerous phenotypes, such as lymphoid and myeloid cell invasion and metastasis.[65,66] Other studies have shown that versican is expressed in numerous ocular tissues, including the ciliary body[27,36,37,39,41,42] (Table 1), where cleavage products of the protein are believed to constitute the versican residues that are active within the vitreous.[38] In a previous study by Passi et al.,[16] radiolabeled versican was incubated with recombinant MMP-2 and MMP-9 and proteolysis was monitored by size-exclusion chromatography. The versican fragments detected by these experiments and their respective molecular weights were not described further. Through protein modeling of the *VCAN* mutation found within our VVR family, we are the first to show an MMP cleavage site within the GAGβ domain of versican that could lead to abnormalities in both matrix modeling as well as interactions with other proteins, ultimately leading to the disease phenotype.

VVR mutations commonly result in defective *VCAN* splicing that results in a partial or full deletion of exon 8, as well as imbalanced levels of versican isoforms (decrease V0/V1 and increased V2/V3 transcript levels). The pedigree described in the current study harbors the canonical *VCAN* splice site mutation (c.4004-2A>G) that introduces a cryptic splice acceptor site in intron 7 resulting in a 39-bp deletion in exon 8 that removes 13 amino acids from the GAGβ chain. Either a haplo-insufficiency of V0 and/or V1 or an imbalance of *VCAN* isoforms comprises a common pathogenic mechanism of VVR mutations known to date; however, the functional consequences of a truncated or deleted exon 8 on versican protein function are poorly understood. We investigated this question further using structural bioinformatic methodologies and identified a novel MMP proteolytic site (VCAN p.1335-1347; NP_004376.2) that is deleted as a result of this canonical splice

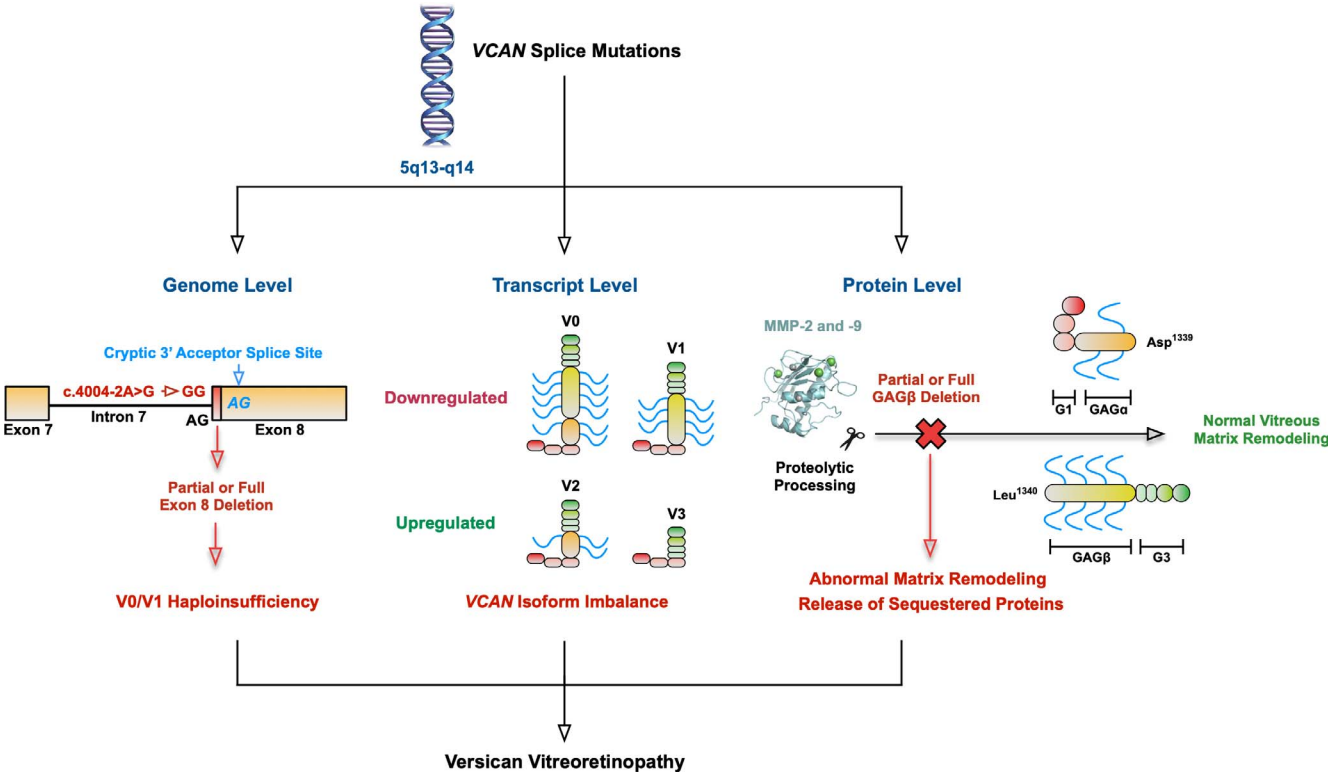

Figure 7. Proposed disease model for versican vitreoretinopathy. Splice site mutations in *VCAN* disrupt proteolytic processing of versican at the protein level, leading to abnormal matrix modeling and release of sequestered proteins from the vitreous hyaluronan network.

mutation. Removal of this MMP site may have important implications on the proteolytic processing of versican and its interactions with binding partners in the vitreous. Taken together, these findings may represent overlapping pathophysiologic mechanisms contributing to the VVR clinical phenotype (Fig. 7).

It remains unclear why the VVR disease phenotype is restricted exclusively to ocular tissues. One possibility is that the V0 and V1 transcripts affected by VVR mutations are more abundant in the eye. Studies have shown that *VCAN* exon 8 splice site variants lead to an imbalance of mRNA isoforms in VVR patients.[1] Each *VCAN* transcript may play a unique role in the eye, and disruption of V0 and V1 may not be easily compensated by increased V2 and V3 expression. Alternatively, it is possible that while versican is critical for the normal embryologic development of the eye, it may be less essential for the development of extraocular tissues.

The absence or truncation of the GAGβ domain may have deleterious effects on VCAN protein function, among which are its interaction with other proteins within the posterior segment. Our network analysis modeling identified numerous nonstructural vitreous proteins whose interactions with normal versican may be disrupted. Of note, FBLN-1 has been known to bind versican to form a major hyaluronan-binding complex that generates cleavage products that are indispensable for the physiologic properties of the vitreous,[67] and disruption of this interaction may underlie the pathophysiology of RD observed in both VVR and Marfan syndrome, a genetic disease due to FBLN-1 dysfunction.[68,69] The network modeling analysis also identified CXCL12 and VEGFA as interacting with versican. CXCL12 is a proinflammatory chemotactic molecule that, when not sequestered by functional versican, can lead to ocular inflammation and uveitis. VEGFA is a growth factor, which is involved in increasing neovascularization, vascular permeability, and PVR formation. These characteristics have all been observed within the members of our VVR family.

There are limitations to the current study. While highly informative, in vitro assays may not reflect the full-length versican protein and physiologic conditions. Future studies are needed to validate VCAN p.1335-1347 as a physiologic MMP cleavage site in the vitreous. Although the canonical *VCAN* splice site mutation is associated with 39-bp deletion in exon 8, we did not perform qRT-PCR analysis of the 39-bp deletion on full blood RNA from our patients to estimate the contribution of this mutant mRNA compared with other mRNA transcripts. Finally, further in vivo studies are necessary to elucidate the downstream molecular pathways activated by the dysregulation of each of these proteins. Therapeutic targeting of these pathways may offer novel methods to mitigate disease.

Acknowledgments

The authors thank Leela Mahajan for surgical drawings, Vishal Perera and Jing Yang for technical assistance, and Nasreen Syed for sharing pathology reports.

Supported by National Institutes of Health (Bethesda, MD, USA) Grants K08EY020530, R01EY024665, R01EY025225, R01EY024698, R21AG050437, P30EY026877 (VBM), Doris Duke Charitable Foundation Grant No. 2013103 (Sanford Burnham Medical Research Institute, La Jolla, CA, USA), Research to Prevent Blindness (New York, NY, USA), and the Stanford ChEM-H Testing Molecular Hypotheses in Human Subjects Seed Grant (Palo Alto, CA, USA). The Barbara & Donald Jonas Laboratory of Regenerative Medicine and Bernard & Shirlee Brown Glaucoma Laboratory are supported by the Congressionally Directed Medical Research Programs TSCRP:TS080017 (Fort Detrick, MD, USA), National Institute of Health (5P30EY019007, R01EY018213, R01EY024698, R01EY026682, R21AG050437); National Cancer Institute Core (5P30CA013696; Bethesda, MD, USA); the Research to Prevent

Blindness Physician-Scientist Award; unrestricted funds from Research to Prevent Blindness; the Tistou and Charlotte Kerstan Foundation (Tübingen, Germany); the Crowley Family Fund (Dallas, TX, USA); the Schneeweiss Stem Cell Fund (Columbia University, New York, NY, USA); New York State (C029572; Albany, NY, USA); and the Gebroe Family Foundation (Albany, NY, USA). GV is supported by NIH grants (F30EYE027986 and T32GM007337).

Disclosure: **P.H. Tang**, None; **G. Velez**, None; **S.H. Tsang**, None; **A.G. Bassuk**, None; **V.B. Mahajan**, None

References

1. Mukhopadhyay A, Nikopoulos K, Maugeri A, et al. Erosive vitreoretinopathy and wagner disease are caused by intronic mutations in CSPG2/Versican that result in an imbalance of splice variants. *Invest Ophthalmol Vis Sci*. 2006;47:3565–3572.
2. Brown DM, Graemiger RA, Hergersberg M, et al. Genetic linkage of wagner disease and erosive vitreoretinopathy to chromosome 5q13-14. *Arch Ophthalmol*. 1995;113:671–675.
3. Kloeckener-Gruissem B, Bartholdi D, Abdou MT, Zimmermann DR, Berger W. Identification of the genetic defect in the original Wagner syndrome family. *Mol Vis*. 2006;12:350–355.
4. Burin-des-Roziers C, Rothschild PR, Layet V, et al. Deletions overlapping VCAN exon 8 are new molecular defects for Wagner disease. *Hum Mutat*. 2017;38:43–47.
5. Perveen R, Hart-Holden N, Dixon MJ, et al. Refined genetic and physical localization of the Wagner disease (WGN1) locus and the genes CRTL1 and CSPG2 to a 2- to 2.5-cM region of chromosome 5q14.3. *Genomics*. 1999;57:219–226.
6. Rothschild PR, Brezin AP, Nedelec B, et al. A family with Wagner syndrome with uveitis and a new versican mutation. *Mol Vis*. 2013;19:2040–2049.
7. Ronan SM, Tran-Viet KN, Burner EL, Metlapally R, Toth CA, Young TL. Mutational hot spot potential of a novel base pair mutation of the CSPG2 gene in a family with Wagner syndrome. *Arch Ophthalmol*. 2009;127:1511–1519.
8. Mukhopadhyay A, Nikopoulos K, Maugeri A, et al. Erosive vitreoretinopathy and wagner disease are caused by intronic mutations in CSPG2/Versican that result in an imbalance of splice variants. *Invest Ophthalmol Vis Sci*. 2006;47:3565–3572.
9. Miyamoto T, Inoue H, Sakamoto Y, et al. Identification of a novel splice site mutation of the CSPG2 gene in a Japanese family with Wagner syndrome. *Invest Ophthalmol Vis Sci*. 2005;46:2726–2735.
10. Kloeckener-Gruissem B, Neidhardt J, Magyar I, et al. Novel VCAN mutations and evidence for unbalanced alternative splicing in the pathogenesis of Wagner syndrome. *Eur J Hum Genet*. 2013;21:352–356.
11. Brezin AP, Nedelec B, Barjol A, Rothschild PR, Delpech M, Valleix S. A new VCAN/versican splice acceptor site mutation in a French Wagner family associated with vascular and inflammatory ocular features. *Mol Vis*. 2011;17:1669–1678.
12. Van Nouhuys CE. Chorioretinal dysplasia in young subjects with Wagner's hereditary vitreoretinal degeneration. *Int Ophthalmol*. 1981;3:67–77.
13. Brown DM, Kimura AE, Weingeist TA, Stone EM. Erosive vitreoretinopathy. A new clinical entity. *Ophthalmology*. 1994;101:694–704.
14. Maumenee IH, Stoll HU, Mets MB. The Wagner syndrome versus hereditary arthroophthalmopathy. *Trans Am Ophthalmol Soc*. 1982;80:349–365.
15. Zhang Z, Miao L, Wang L. Inflammation amplification by Versican: the first mediator. *Int J Mol Sci*. 2012;13:6873–6882.
16. Passi A, Negrini D, Albertini R, Miserocchi G, De Luca G. The sensitivity of versican from rabbit lung to gelatinase A (MMP-2) and B (MMP-9) and its involvement in the development of hydraulic lung edema. *FEBS Lett*. 1999;456:93–96.
17. Stanton H, Melrose J, Little CB, Fosang AJ. Proteoglycan degradation by the ADAMTS family of proteinases. *Biochim Biophys Acta*. 2011;1812:1616–1629.
18. McCulloch DR, Nelson CM, Dixon LJ, et al. ADAMTS metalloproteases generate active versican fragments that regulate interdigital web regression. *Dev Cell*. 2009;17:687–698.
19. Nandadasa S, Foulcer S, Apte SS. The multiple, complex roles of versican and its proteolytic turnover by ADAMTS proteases during embryogenesis. *Matrix Biol*. 2014;35:34–41.
20. Kloeckener-Gruissem B, Dours-Zimmermann MT, Skosyrski S, et al. A potential mouse model for the erosive vitreoretinopathy of Wagner disease. *Matters*. 2016;2:e201605000004.
21. Popp S, Maurel P, Andersen JS, Margolis RU. Developmental changes of aggrecan, versican and neurocan in the retina and optic nerve. *Exp Eye Res*. 2004;79:351–356.
22. Wolf LV, Yang Y, Wang J, et al. Identification of pax6-dependent gene regulatory networks in the mouse lens. *PLoS One*. 2009;4:e4159.
23. Benke K, Agg B, Szilveszter B, et al. The role of transforming growth factor-beta in Marfan syndrome. *Cardiol J*. 2013;20:227–234.
24. Miyamoto T, Inoue H, Sakamoto Y, et al. Identification of a novel splice site mutation of the CSPG2 gene in a Japenese family with Wagner syndrome. *Invest Ophthalmol Vis Sci*. 2005;46:2726–2735.
25. Ankala A, Jain N, Hubbard B, Alexander JJ, Shankar SP. Is exon 8 the most critical or the only dispensable exon of the VCAN gene? Insights into VCAN variants and clinical spectrum of Wagner syndrome. *Am J Med Genet A*. 2018;176:1778–1783.
26. Skeie JM, Mahajan VB. Proteomic interactions in the mouse vitreous-retina complex. *PLoS One*. 2013;8:e82140.
27. Skeie JM, Roybal CN, Mahajan VB. Proteomic insight into the molecular function of the vitreous. *PLoS One*. 2015;10:e0127567.
28. Velez G, Tsang SH, Tsai YT, et al. Gene therapy restores Mfrp and corrects axial eye length. *Sci Rep*. 2017;7:16151.
29. Kumar S, Ratnikov BI, Kazanov MD, Smith JW, Cieplak. CleavPredict: a platform for reasoning about matrix metalloproteinases proteolytic events. *PLoS One*. 2015;10:e0127877.
30. Rawlings ND, Barrett AJ, Bateman A. MEROPS: the peptidase database. *Nucleic Acids Res*. 2010;38:D227–D233.
31. Trott O, Olson AJ. AutoDock Vina: improving the speed and accuracy of docking with a new scoring function, efficient optimization, and multithreading. *J Comput Chem*. 2010;31:455–461.
32. Velez G, Machlab DA, Tang PH, et al. Proteomic analysis of the human retina reveals region-specific susceptibilities to metabolic- and oxidative stress-related diseases. *PLoS One*. 2018;13:e0193250.
33. Szklarczyk D, Franceschini A, Wyder S, et al. STRING v10: protein-protein interaction networks, integrated over the tree of life. *Nucleic Acids Res*. 2015;43:D447–D452.
34. Xia J, Gill EE, Hancock RE. NetworkAnalyst for statistical, visual and network-based meta-analysis of gene expression data. *Nat Protoc*. 2015;10:823–844.
35. Shannon P, Markiel A, Ozier O, et al. Cytoscape: a software environment for integrated models of biomolecular interaction networks. *Genome Res*. 2003;13:2498–2504.
36. Koga T, Inatani M, Hirata A, et al. Expression of a chondroitin sulfate proteoglycan, versican (PG-M), during development of rat cornea. *Curr Eye Res*. 2005;30:455–463.
37. Ueda J, Yue BY. Distribution of myocilin and extracellular matrix components in the corneoscleral meshwork of human eyes. *Invest Ophthalmol Vis Sci*. 2003;44:4772–4779.

38. Ohno-Jinno A, Isogai Z, Yoneda M, et al. Versican and fibrillin-1 form a major hyaluronan-binding complex in the ciliary body. *Invest Ophthalmol Vis Sci*. 2008;49:2870–2877.
39. Carnes MU, Allingham RR, Ashley-Koch A, Hauser MA. Transcriptome analysis of adult and fetal trabecular meshwork, cornea, and ciliary body tissues by RNA sequencing. *Exp Eye Res* 2018;167:91–99.
40. Uhlen M, Fagerberg L, Hallstrom BM, et al. Proteomics. Tissue-based map of the human proteome. *Science*. 2015;347:1260419.
41. Skeie JM, Mahajan VB. Proteomic landscape of the human choroid-retinal pigment epithelial complex. *JAMA Ophthalmol*. 2014;132:1271–1281.
42. Cabral T, Toral MA, Velez G, et al. Dissection of human retina and RPE-choroid for proteomic analysis. *J Vis Exp*. 2017;129: e56203.
43. Wight TN. Versican: a versatile extracellular matrix proteoglycan in cell biology. *Curr Opin Cell Biol*. 2002;14:617–623.
44. Wu YJ, La-Pierre DP, Wu J, Yee AJ, Yang BB. The interaction of versican with its binding partners. *Cell Res*. 2005;15:483–494.
45. Theocharis DA, Skandalis SS, Noulas AV, Papageorgakopoulou N, Theocharis AD, Karamanos NK. Hyaluronan and chondroitin sulfate proteoglycans in the supramolecular organization of the mammalian vitreous body. *Connect Tissue Res*. 2008; 49:124–128.
46. Bishop PN. Structural macromolecules and supramolecular organisation of the vitreous gel. *Prog Retin Eye Res*. 2000;19: 323–344.
47. Bassuk AG, Yeh S, Wu S, et al. Structural modeling of a novel CAPN5 mutation that causes uveitis and neovascular retinal detachment. *PLoS One*. 2015;10:e0122352.
48. Cox AJ, Darbro BW, Laxer RM, et al. Recessive coding and regulatory mutations in FBLIM1 underlie the pathogenesis of chronic recurrent multifocal osteomyelitis (CRMO). *PLoS One*. 2017;12:e0169687.
49. Moshfegh Y, Velez G, Li Y, Bassuk AG, Mahajan VB, Tsang SH. BESTROPHIN1 mutations cause defective chloride conductance in patient stem cell-derived RPE. *Hum Mol Genet*. 2016; 25:2672–2680.
50. Toral MA, Velez G, Boudreault K, et al. Structural modeling of a novel SLC38A8 mutation that causes foveal hypoplasia. *Mol Genet Genomic Med*. 2017;5:202–209.
51. Velez G, Bassuk AG, Schaefer KA, et al. A novel de novo CAPN5 mutation in a patient with inflammatory vitreoretinopathy, hearing loss, and developmental delay. *Cold Spring Harb Mol Case Stud*. 2018;4.a002519.
52. Velez G, Tsang S, Tsai Y, et al. Gene therapy restores mfrp and corrects axial eye length. *Sci Rep*. 2017;7:16151.
53. Fields GB. Using fluorogenic peptide substrates to assay matrix metalloproteinases. *Methods Mol Biol*. 2010;622:393–433.
54. Nagase H, Suzuki K, Morodomi T, Enghild JJ, Salvesen G. Activation mechanisms of the precursors of matrix metalloproteinases 1, 2 and 3. *Matrix Suppl*. 1992;1:237–244.
55. Ruoslahti E, Yamaguchi Y. Proteoglycans as modulators of growth factor activities. *Cell*. 1991;64:867–869.
56. Doyle JJ, Gerber EE, Dietz HC. Matrix-dependent perturbation of TGFbeta signaling and disease. *FEBS Lett*. 2012;586:2003–2015.
57. Wu YJ, La Pierre DP, Wu J, Yee AJ, Yang BB. The interaction of versican with its binding partners. *Cell Res*. 2005;15:483–494.
58. Reinhard J, Renner M, Wiemann S, et al. Ischemic injury leads to extracellular matrix alterations in retina and optic nerve. *Sci Rep*. 2017;7:43470.
59. Kawashima H, Atarashi K, Hirose M, et al. Oversulfated chondroitin/dermatan sulfates containing GlcAbeta1/IdoAalpha1-3GalNAc(4,6-O-disulfate) interact with L- and P-selectin and chemokines. *J Biol Chem*. 2002;277:12921–12930.
60. Fu Y, Nagy JA, Brown LF, et al. Proteolytic cleavage of versican and involvement of ADAMTS-1 in VEGF-A/VPF-induced pathological angiogenesis. *J Histochem Cytochem*. 2011;59: 463–473.
61. Pennock AT, Alam M, Bastrom T. Variation in tibial tubercle-trochlear groove measurement as a function of age, sex, size, and patellar instability. *Am J Sports Med*. 2014;42:389–393.
62. Mohan N, Monickaraj F, Balasubramanyam M, Rema M, Mohan V. Imbalanced levels of angiogenic and angiostatic factors in vitreous, plasma and postmortem retinal tissue of patients with proliferative diabetic retinopathy. *J Diabetes Complications*. 2012;26:435–441.
63. Wight TN. Provisional matrix: a role for versican and hyaluronan. *Matrix Biol*. 2017;60-61:38–56.
64. Wight TN, Kang I, Merrilees MJ. Versican and the control of inflammation. *Matrix Biol*. 2014;35:152–161.
65. Keire PA, Bressler SL, Lemire JM, et al. A role for versican in the development of leiomyosarcoma. *J Biol Chem*. 2014;289: 34089–34103.
66. Du WW, Yang W, Yee AJ. Roles of versican in cancer biology—tumorigenesis, progression and metastasis. *Histol Histopathol*. 2013;28:701–713.
67. Ohno-Jinno A, Isoqai Z, Yoneda M, et al. Versican and fibrillin-1 form a major hyaluronan-binding complex in the ciliary body. *Invest Ophthalmol Vis Sci*. 2008;49:2870–2877.
68. Ramachandra CJ, Mehta A, Guo KW, Wong P, Tan JL, Shim W. Molecular pathogenesis of Marfan syndrome. *Int J Cardiol*. 2015;187:585–591.
69. Verstraeten A, Alaerts M, Van-Laer L, Loeys B. Marfan syndrome and related disorders: 25 years of gene discovery. *Hum Mutat*. 2016;37:524–531.

Investigative Ophthalmology & Visual Science